Project: COVID-19 Assisted Diagnosis

Carlo Heemeryck[1]   Willem Van Nieuwenhuyse[1]   Seppe Vanrietvelde[2]   Luca Visser[2]

[1] Bachelor of Science in de ingenieurswetenschappen - werktuigkunde-elektrotechniek
[2] Master of Science in Statistical Data Analysis - Computational Statistics

I. Introduction

The outbreak of the COVID-19 pandemic in late 2019 has placed unprecedented strain on healthcare systems worldwide, highlighting the urgent need for rapid and accurate diagnostic tools to support clinical decision–making. Chest X-ray imaging has emerged as a widely available modality for the preliminary screening of COVID-19 pneumonia, yet visual assessment alone can be time-consuming and prone to inter-observer variability [1], [2]. In this work, a deep learning–based framework for assisted diagnosis of COVID-19 from chest X-ray images is presented, leveraging both custom convolutional neural networks and transfer learning approaches.

Section II covers exploring the publicly available dataset, detailing the preprocessing pipeline (downsampling, normalization, and light augmentation) and presenting initial sample images (Fig. 1). In Section III, a baseline CNN model is build and evaluated, reporting its architecture (Table I), learning curves (Fig. ??), and test-set performance including a confusion matrix (Fig. 6). Section IV introduces transfer learning with a pre-trained ResNet50V2 backbone, describing model adaptations, hyperparameter tuning, and comparative results. Section V demonstrates model interpretability using Grad-CAM heatmaps, and finally Section VI summarizes the conclusions and outlines potential future work.

II. Task 1: Data Exploration, Pre-Processing and Augmentation

A. Loading the data

The grayscale chest X-ray images are loaded at their original resolution of 299×299 pixels. The labels, either COVID or NORMAL, are taken from the folder names containing the images and assumed to be accurate. From the outset, the dataset was pre-divided into training (1,600 images), validation (400 images), and test (200 images) sets. This original distribution is preserved for the exercise, with an additional combined training and validation set comprising 2,000 images.

B. Data exploration

Exploration consists of checking the shape of the data, evaluating the distribution of the two classes, plotting a few examples and checking pixel and global average and standard deviation. This is replicated for training, validation and test datasets and serves as an initial look at the data and to possibly detect problems at an early stage in the project. All the images in the training dataset are of the same size and there are an equal amount in both classes, which is good. A few labeled examples are given in Fig. 1.
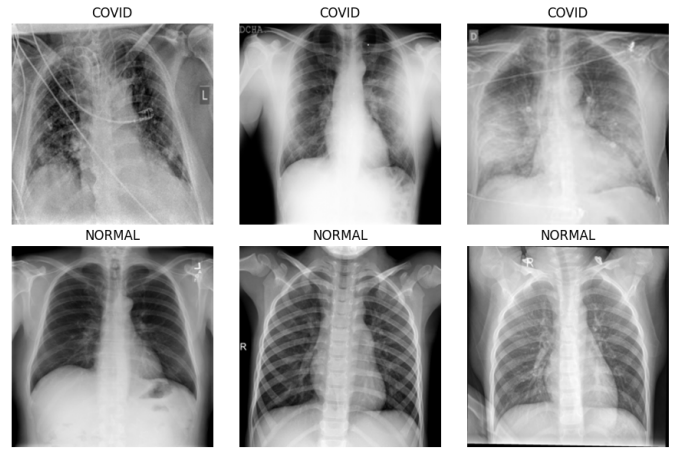

Fig. 1. A few images from the training dataset with accompanying labels.

There seem to be no clear differences between the NORMAL and COVID images. However, the limitation to grayscale images, low contrasts, different zoom levels and slight variations in angles could be problems for classification. Also if there are, to us unrecognisable, artifacts in mostly one category, generalization to new images could be problematic. Over all images in the training dataset the average value and the standard deviation at every pixel location can be visualized to show a sort of average image and a heatmap for variation. These visualizations, together with the average and standard deviation of all pixels, are given in Fig. 2.

Replicating all this for the validation and test datasets give very comparable results, indicating that the images were uniformly divided over the different sets. The exploration of the validation and test sets can be consulted in the notebook.
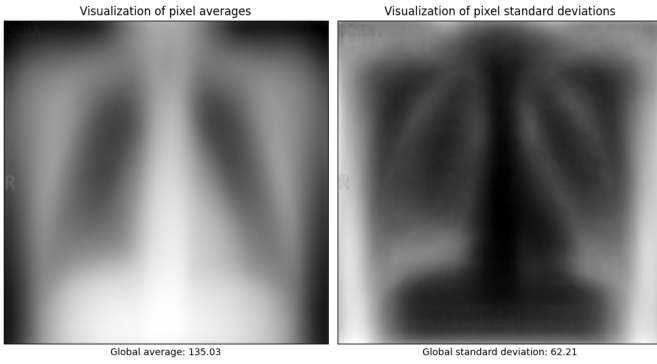
Fig. 2. A visualization of the average image (left) and a variation heatmap (right) with accompanying global statistics from the training dataset.

C. Pre-processing

Next, some pre-processing steps are implemented and evaluated, namely down sampling to 128 x 128 pixels using bilinear interpolation and a few normalization strategies. The result of down sampling, given in Fig. 3, is still recognisable to the human eye. As such, it is assumed that the model still gets enough information from this. Implementing this down sampling strategy should reduce training time while not losing too much performance.
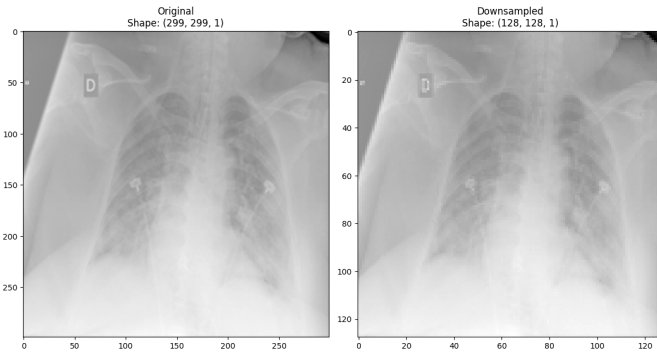

Fig. 3. An example of a downsampled image using bilinear interpolation (299x299 -> 128x128).

Normalization through the use of a fixed value (dividing by 255), sample statistics (subtracting the overall mean and dividing by the overall standard deviation of the current sample (training, validation or test)) and statistics of the training dataset (subtracting the overall mean and dividing by the overall standard deviation of the training dataset) were tried out. All of these strategies resulted in visually the same image but with pixel values with a far lower magnitude. However, normalizing using training set-wide image statistics (mean and std) and applying the same normalization across all images is the most correct method as it causes no data leakage. Normalization based on the training dataset will thus be used in the project.

D. Augmentation

Finally, based on the variety of the plotted images a few augmentation strategies are implemented, namely randomly altering the brightness and the contrast by a factor between 0.6 and 1.4 and randomly rotating the images (anti)clockwise up to 30°. Examples of these augmentation are given in Fig. 4.
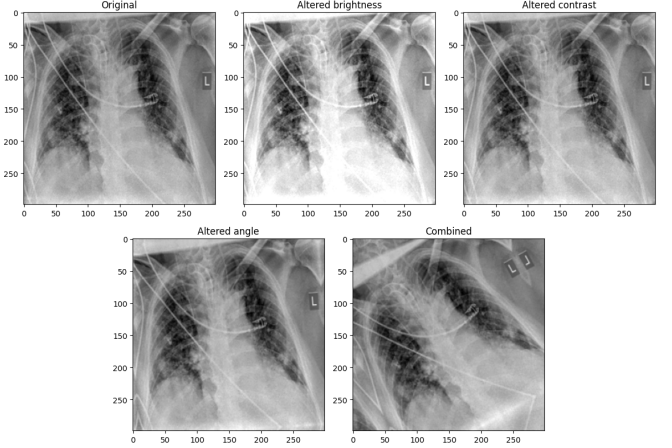

Fig. 4. Examples of different transformations as well as the combination of them together.

Augmentation should only result in images that could occur in test/unseen data. Based on the data we have, intense augmentation doesn't seem al that necessary. It will thus only be considered if necessary.

E. Pipeline

A pipeline consisting of loading the images correctly, with optional downsampling, followed by optional normalization using the training dataset is implemented for later use. Data augmentations can be used as layers in the models if necessary.

III. Task 2: Building the Baseline Model

This section describes the construction, training, and evaluation of an initial convolutional neural network (CNN) model for COVID-19 detection from chest X-ray images. Starting with outlining the model architecture, then proceeding to tuning hyperparameters, and concluding with a performance analysis on the validation and test sets.

A. Initial Model Architecture

A custom CNN with the following components is implemented:

- Input layer: $128 \times 128 \times 1$ grayscale image
- Convolutional blocks: three blocks with increasing filter sizes {16, 32, 64}, each block consists of a

3×3 convolution, ReLU activation, max-pooling, and dropout (rate 0.1)

- Fully connected layer: 512 units with ReLU activation and dropout (rate 0.1)
- Output layer: single unit with sigmoid activation for binary classification

A summary of the full architecture is shown in Table I.

TABLE I
Initial Baseline CNN Architecture Overview.

Layer (type)	Output Shape	# Params
Conv2D (3×3, 16 filters)	(None, 128, 128, 16)	160
MaxPooling2D (2×2)	(None, 64, 64, 16)	0
Dropout (rate = 0.1)	(None, 64, 64, 16)	0
Conv2D_1 (3×3, 32 filters)	(None, 64, 64, 32)	4,640
MaxPooling2D_1 (2×2)	(None, 32, 32, 32)	0
Conv2D_2 (3×3, 64 filters)	(None, 32, 32, 64)	18,496
MaxPooling2D_2 (2×2)	(None, 16, 16, 64)	0
Dropout_1 (rate = 0.1)	(None, 16, 16, 64)	0
Flatten	(None, $16 \cdot 16 \cdot 64 = 16384$)	0
Dense (512 units)	(None, 512)	8,389,120
Dense_1 (1 unit, sigmoid)	(None, 1)	513
Total parameters		8,412,929
Trainable parameters		8,412,929
Non-trainable parameters		0

B. Training Procedure

The model is initially trained on batch sizes of 32 using a learning rate of 10^{-3} using the Adam optimizer on a binary cross-entropy loss function and accuracy as the metric of choice.

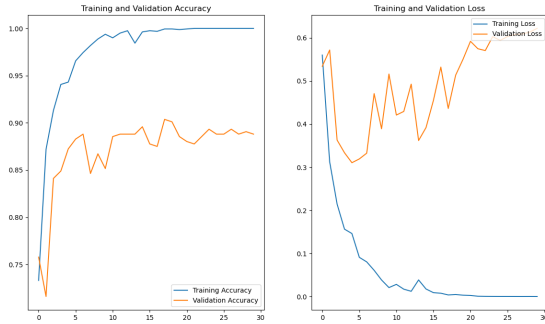The learning curves, spanning 30 epochs, are depicted in Fig. 5.

Fig. 5. Training and validation accuracy and loss for the baseline CNN over 30 epochs.

C. Hyperparameter Tuning

A grid search (with early stopping) was performed over the following hyperparameters:

- Dropout rate: {0.1, 0.2}
- Initial convolutional filters: {8, 16}
- Learning rate: {1e-3, 5e-4}
- Dense units: {256, 512}

The best configuration achieved a validation accuracy of 0.8932 with a dropout rate of 0.2, 8 filters, a learning rate of $\mathbf{10^{-3}}$, and 512 dense units. All results are shown in Table II.

TABLE II
Hyperparameter Tuning Results (sorted by validation accuracy).

Dropout	Filters	LR	Dense Units	Val Acc	Epoch	Val Loss
0.2	8	1e-3	512	0.8932	9	0.2984
0.2	16	1e-3	256	0.8906	7	0.2998
0.1	16	5e-4	512	0.8828	6	0.2970
0.1	8	1e-3	512	0.8828	12	0.3483
0.1	8	1e-3	256	0.8776	8	0.3139
0.1	16	1e-3	512	0.8724	5	0.3096
0.2	16	5e-4	256	0.8698	9	0.3422
0.2	8	5e-4	512	0.8698	10	0.2969
0.2	16	5e-4	512	0.8672	4	0.3052
0.1	8	5e-4	512	0.8646	12	0.3483
0.2	16	1e-3	512	0.8646	6	0.3223
0.1	16	1e-3	256	0.8620	4	0.3276
0.2	8	5e-4	256	0.8620	8	0.3166
0.1	8	5e-4	256	0.8594	8	0.3343
0.2	8	1e-3	256	0.8464	5	0.3387
0.1	16	5e-4	256	0.8385	5	0.3608

D. Final Baseline Model

Using the best hyperparameters, the model was re-trained on the training and validation sets together (2,000 images) for 8 epochs. Evaluation on the held-out test set (200 images) yielded:

- Test accuracy: 0.8300
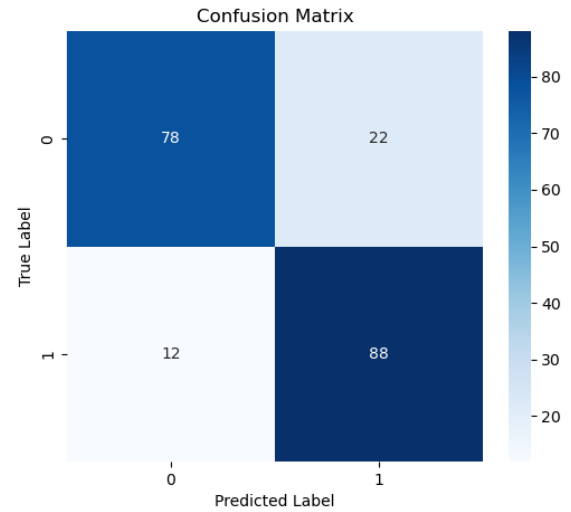- Test loss: 0.3835

The confusion matrix is shown in Fig. 6.

Fig. 6. Confusion matrix of the final baseline model on the test set (1: NORMAL, 0: COVID).

E. Discussion

The baseline model achieved 83% accuracy, demonstrating strong discriminative power between COVID-19 and normal chest X-ray images. The following is observed from the confusion matrix (Fig. 6):

- True negatives (NORMAL correctly classified): 88
- False positives (NORMAL misclassified as COVID): 12
- False negatives (COVID misclassified as NORMAL): 22
- True positives (COVID correctly classified): 78

This yields a sensitivity (recall for COVID) of $78/(78 + 22) = 0.78$ and a specificity of $88/(88 + 12) = 0.88$. The slightly higher sensitivity indicates that the model is more likely to correctly detect COVID cases, at the cost of some false alarms.

In our final training run—conducted without a separate validation split—we noted that training loss continued to decline predictably with each epoch. However, without a validation curve to signal overfitting, determining the optimal early-stopping point became speculative. In future work, reintroducing a validation set or implementing cross-validation will be essential to choose the right number of epochs.

The training curves, shown in Fig. 5, suggest rapid convergence of training accuracy to nearly 100% within the first 10 epochs, while validation accuracy plateaus around 88%, suggesting that there is still some overfitting, even after controlling via dropout. Overall, the baseline CNN provides a solid starting point.

IV. Task 3: Transfer Learning

In this task transfer learning by using a pre-trained ResNet50V2 model trained on Imagenet is applied. Transfer learning is a powerful machine learning technique for leveraging knowledge learned from one task and applying it to a new task. This is especially useful when you have limited training data.

The typical workflow for transfer learning is as follows:

1) Start with a pretrained model
2) Freeze the layers of the pretrained model
3) Add new trainable layers to the pretrained model
4) Train on the dataset
5) Fine-tuning (optional)

The layers of the pretrained model are frozen to prevent elementary information learned from the initial task from being overwritten during the new training process. New layers are added to the pretrained model to adapt it to the new task, which need to be trained on new data. Optionally, the last layers of the original model can be unfrozen and retrained to fine-tune the model even more.

A. Setup of the base model

The base model (ResNet50V2) is instantiated with the "imagenet" pre-trained weights, not including the top layers. All the layers of the base model are frozen so their weights are not updated during the training process. Then, new fully connected layers are added to the model with dropout in between (Table III). The architecture of the final layers added to the pre-trained model are exactly the same as the fully connected layers of the baseline model.

TABLE III
Initial Transfer Model Architecture

Layer (type)	Output Shape	# Params
augmentation	(None, 128, 128, 3)	0
ResNet50V2 (pre-trained)	(None, 4, 4, 2048)	23,564,800
Dropout (rate = 0.1)	(None, 4, 4, 2048)	0
GlobalAveragePooling2D	(None, 2048)	0
Dense (256 units)	(None, 256)	524,544
Dropout (rate = 0.1)	(None, 256)	0
Dense (256 units)	(None, 256)	65,792
Dropout (rate = 0.1)	(None, 256)	0
Dense_1 (1 unit, sigmoid)	(None, 1)	257
Total parameters		24,155,393
Trainable parameters		590,593
Non-trainable parameters		23,564,800

B. Training procedure

The model is initially trained using the best hyperparameters found while tuning the baseline model in the previous section, again using the Adam optimizer on a binary cross-entropy loss function and accuracy as the metric of choice.

The learning curves, spanning 30 epochs, are depicted in Fig. 7.

Fig. 7. Training and validation accuracy and loss for the initial transfer learning model over 30 epochs.

The model trains without errors and the loss stabilizes somewhat but the results are clearly worse.

C. Hyperparameter tuning

A grid search (with early stopping) was performed over the following hyperparameters:

- Dropout rate: {0.1, 0.2, 0.3}

- Learning rate: {1e-3, 5e-4}
- Batch size: {32, 64}

The best configuration achieved a validation accuracy of 1.0000 with a dropout rate of 0.1, a learning rate of 1×10^{-3}, and a batch size of 64.

D. Final transfer learning model

Using the best hyperparameters, the model was retrained on the training and validation sets together (2000 images) for 2 epochs.

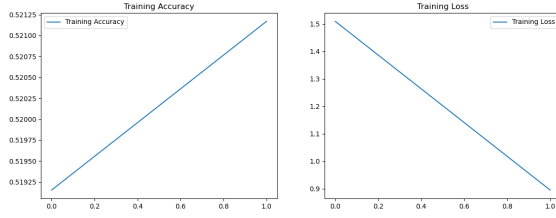the learning curves, spanning 2 epochs, are depicted in Fig. 8.

Fig. 8. Training accuracy and loss for the final transfer learning model over 2 epochs.

E. Fine-tuning

In this step all of the base model layers are unfrozen. The whole model is completely retrained using the training and validation set together.

Evaluation on the held-out test set (200 images) yielded:
- Accuracy: 83.5%
- Loss: 0.6901

The model clearly performs better than the pre-trained model. This could be expected because the model is now completely trained on our own data.

The confusion matrix is shown in Fig. 9.

Finally a few images are plotted from the test dataset in Fig. 10. First without pre-processing, then with their evaluations after pre-processing.

F. Discussion

The following is observed from the confusion matrix (Fig. 9):
- True negatives (NORMAL correctly classified): 84
- False positives (NORMAL misclassified as COVID): 17
- False negatives (COVID misclassified as NORMAL): 16
- True positives (COVID correctly classified): 83

This yields a sensitivity (recall for COVID) of $83/(83 + 17) = 0.83$ and a specificity of $84/(84+16) = 0.84$. Overall, the model performs reasonably well but could still benefit from reducing false positives and false negatives.
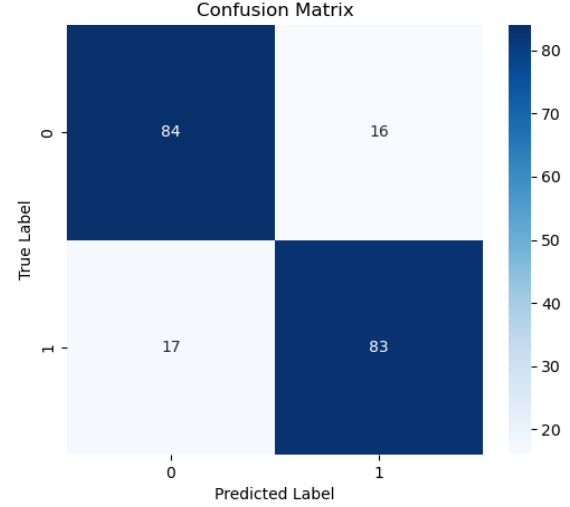

Fig. 9. Confusion matrix for the fine-tuned transfer learning model (1: NORMAL, 0: COVID).
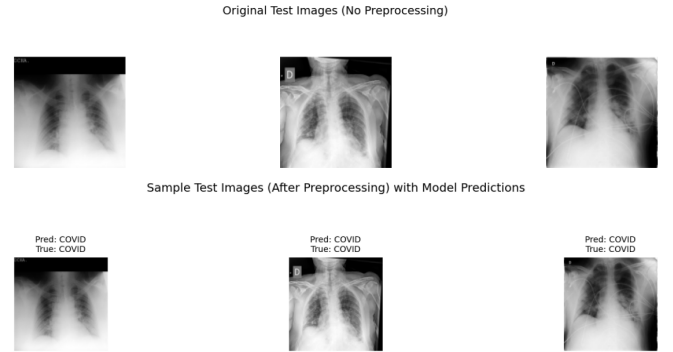

Fig. 10. Test Samples with and without pre-processing and there labels.

The results are very similar as the baseline model. But being more complex makes it less preferred.

From this experience, it can be concluded that transfer learning has both advantages and disadvantages. On the positive side, training was faster given the same amount of data. On the negative side, the base model and its pretrained weights may not have been well-suited for the task at hand, making fine-tuning a delicate and challenging process.

To improve the effectiveness of transfer learning in this context, several modifications could be considered. Notably, the base model was pretrained on RGB images of various objects, which differs significantly from the grayscale medical images used in our task. Using a pretrained model that was trained on data more similar to our target domain could yield better results and enhance the overall performance of the transfer learning approach.
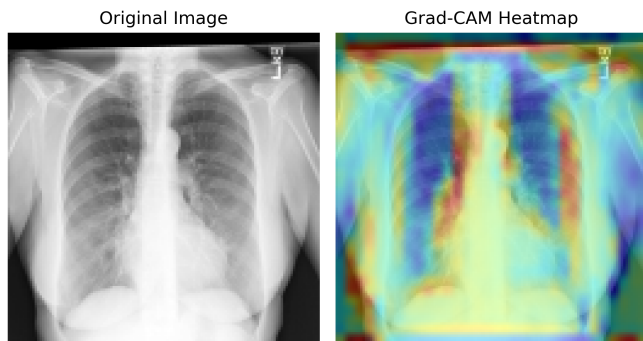
Fig. 11. Grad CAM test image.

V. Task 4: Explainability through Grad-CAM

VI. Conclusions

Our preprocessing pipeline's success in preserving diagnostic detail while standardizing inputs means the model is learning from consistent, clinically relevant features rather than spurious artifacts. By downsampling images to 128×128, we struck a balance between computational efficiency and preserving the lung patterns critical for detecting COVID-19 infiltrates. The uniform distribution across dataset splits—and the fact that light augmentations did not introduce unrealistic distortions—suggests that our model will be resilient to variations in real-world chest X-ray quality (different machines, exposure settings, and patient positioning), reducing the risk that it will latch onto dataset-specific quirks rather than true pathology.

Moving to the baseline CNN, reaching high sensitivity with somewhat lower specificity highlights an important clinical trade-off: the model is tuned to minimize missed COVID-19 cases (false negatives), which is crucial in a screening context, even at the cost of some false positives. This means in practice, our tool could flag more scans for follow-up rather than risk overlooking an infected patient, aligning with a conservative screening philosophy. The rapid convergence and plateauing of validation performance indicate that our architecture is powerful enough to capture discriminative patterns but also that future gains will likely come not from making the network deeper, but from richer data (additional cases, varied sources) or from integrating more advanced techniques like transfer learning and interpretability methods to further refine what the model "looks at" in each X-ray.

VII. Author contributions and collaboration

In our group-based collaboration, each member took primary responsibility for one of the four major tasks—Seppe led Task 1 (Data Exploration and Pre-Processing),

Luca developed Task 2 (Baseline Model Architecture), Willem implemented Task 3 (Transfer Learning), and Carlo focused on Task 4 (Grad-CAM Explainability)—while all four contributed together to framing the introduction, discussion, and conclusion. Throughout the project, we regularly cross-reviewed each other's code, methodologies, and report drafts to ensure consistency, correctness, and clarity, stepping in to proofread and validate results beyond our individual assignments.

VIII. Use of Generative AI

In this project, Practical 3 served as the foundational template for Tasks 1 & 2—providing the baseline model architecture, image-generation pipeline, and core preprocessing routines—while ChatGPT and GitHub Copilot were primarily leveraged to tidy up code, help identify bugs, and offer small implementation suggestions. Neither tool was purposefully relied upon to devise fundamentally new methodologies or novel, overly complex model designs beyond the scope of the course.

For the written report, ChatGPT was also used sparingly to automate repetitive formatting tasks such as inserting tables and to perform spell-checking and grammar refinement suggestions, ensuring consistency and polish without supplanting the original content.

A. Figures and Tables

a) Positioning Figures and Tables: All figures and tables are inserted using the placement specifier [htbp]; each graphic is scaled to the column width via \includegraphics[width=\linewidth]{…}, centered in its float, and accompanied by a concise caption via \caption{…}. We reference every float in the text (e.g., "Fig. X" or "Table Y") and rely on the class's default top-of-column placement to maintain formatting consistency.

References

[1] Wang, L., Lin, Z. Q., & Wong, A. (2020). Covid-net: A tailored deep convolutional neural network design for detection of covid-19 cases from chest x-ray images. Scientific reports, 10(1), 19549.
[2] Apostolopoulos, I. D., & Mpesiana, T. A. (2020). Covid-19: automatic detection from x-ray images utilizing transfer learning with convolutional neural networks. Physical and engineering sciences in medicine, 43, 635-640.